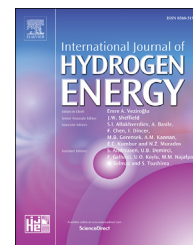




ELSEVIER

Available online at [www.sciencedirect.com](http://www.sciencedirect.com)

ScienceDirect

journal homepage: [www.elsevier.com/locate/ijhe](http://www.elsevier.com/locate/ijhe)

# The effects of Co/Ce loading ratio and reaction conditions on CDRM performance of Co–Ce/ZrO<sub>2</sub> catalysts

A. Ipek Paksoy<sup>a,b</sup>, Burcu Selen Caglayan<sup>b,c</sup>, Emrah Ozensoy<sup>d</sup>, A.N. Ökte<sup>e</sup>,  
A. Erhan Aksoylu<sup>a,b,\*</sup>

<sup>a</sup> Department of Chemical Engineering, Bogazici University, 34342, Bebek, İstanbul, Turkey

<sup>b</sup> SNG&HydTec Lab, Bogazici University, İstanbul, Turkey

<sup>c</sup> Advanced Technologies R&D Center, Bogazici University, 34342, Bebek, İstanbul, Turkey

<sup>d</sup> Department of Chemistry, Bilkent University, 06800, Ankara, Turkey

<sup>e</sup> Department of Chemistry, Bogazici University, 34342, Bebek, İstanbul, Turkey

## ARTICLE INFO

### Article history:

Received 22 September 2017

Received in revised form

26 December 2017

Accepted 1 January 2018

Available online 9 February 2018

### Keywords:

Methane dry reforming

CO<sub>2</sub> utilization

Catalytic H<sub>2</sub> production

Non-PGM catalyst

## ABSTRACT

This work mainly aims to establish a link between Co/Ce loading ratio in Co–Ce/ZrO<sub>2</sub> catalysts and their Carbon Dioxide Reforming of Methane (CDRM) performance. In this context, catalysts with different Co and Ce loadings were prepared and characterized via BET, XRD, HRTEM-EDX, XPS and Raman, and parametrically tested under different CDRM conditions. Dispersion of Co particles was nonhomogeneous on all samples. For the sample with the highest Co/Ce ratio (10%Co–2%Ce/ZrO<sub>2</sub>), higher amount of lattice oxygen vacancies and lowest degree of ceria reduction were determined. Raman analysis showed that graphitic carbon coexisted with amorphous carbon on the surface of all spent samples. The extent of side reactions prevailed in determining selectivity. It was expressed that both Co–Ce synergistic interaction and synchronous contribution of Ce and ZrO<sub>2</sub> were enhanced for the samples having lower Co/Ce ratio. It was confirmed that Ce is only responsible for oxygen transfer but not its formation.

© 2018 Hydrogen Energy Publications LLC. Published by Elsevier Ltd. All rights reserved.

## Introduction

IPCC 5th assessment report stated that warming of the climate system is unequivocal, and since 1950s, many of the observed changes are unprecedented over decades to millennia. Cumulative anthropogenic emissions of CO<sub>2</sub> largely determine global mean surface warming by the late 21st century and beyond. As CO<sub>2</sub> sequestration both in land and ocean has its own disadvantages and dangers, CO<sub>2</sub>

capture in large point sources and utilizing it in production of valuable chemicals has been accepted as one of the best alternatives in emission mitigation. Carbon dioxide reforming of methane (CDRM), a catalytic process utilizing CO<sub>2</sub> and CH<sub>4</sub> to produce synthesis gas, a value-added product used in producing synthetic fuels and methanol via reactions including Fischer-Tropsch synthesis, has received considerable attention lately [1]. Compared to other routes of indirect CH<sub>4</sub> utilization, such as steam reforming and partial oxidation, the

\* Corresponding author. Department of Chemical Engineering, Bogazici University, 34342, Bebek, İstanbul, Turkey.

E-mail address: [aksoylu@boun.edu.tr](mailto:aksoylu@boun.edu.tr) (A.E. Aksoylu).

<https://doi.org/10.1016/j.ijhydene.2018.01.009>

0360-3199/© 2018 Hydrogen Energy Publications LLC. Published by Elsevier Ltd. All rights reserved.

most important advantage of CDRM is the consumption of thermodynamically stable greenhouse gas, CO<sub>2</sub>. The raw natural gas, whose CO<sub>2</sub> concentration might reach up to 70%, can even be directly used in CDRM to save from subsequent gas separation and purification processes [2]. Moreover, obtained H<sub>2</sub>/CO product ratio is closer to 1, which is preferable for further processes like Fischer-Tropsch synthesis. Due to the endothermic nature of the reaction, CDRM can be also used in areas like a system for solar energy transfer to chemical energy, energy storage in the form of CO and H<sub>2</sub> and in chemical energy transmission systems [3]. The main drawback of this process is catalyst deactivation due to carbon deposition from CH<sub>4</sub> decomposition and/or Boudouard reaction; thus, the challenge is to promote CDRM with a very low coke formation rate [4]. Additional problems that may be encountered are metal sintering due to high reaction temperatures, and reverse water-gas shift reaction which leads to H<sub>2</sub>/CO ratio lower than the appropriate value, 1 [4–6].

Since in general coking and metal sintering occur simultaneously, some methods focus on inhibition of both [7]. One of these methods is to synthesize complex solids with well-defined characteristics; in which the ability to produce samples with specific sizes or shapes, or to grow complex solid nanostructures yields to fulfill specific requirements of catalysis in terms of selectivity and stability [7]. Encapsulation strategy, which includes the introduction of a coating to stabilize the active metal species in catalysts, is the other proposed method in literature. However, this process can become disadvantageous since mass transfer might become limited by the encapsulation structure to some extent [8].

Carbon formation and coke deposition on a CDRM catalyst can be controlled by using suitable support, metal and promoter combination(s). The primary properties of supports are their surface area, acid-base nature and ability to disperse the supported phase [9]. A support that favors CO<sub>2</sub> dissociation reaction, by which surface oxygen necessary to clean carbon away from the metallic surface is produced, can be utilized for eliminating coking problems [10]. It was also stated that metal-support synergistic effect is beneficial in achieving coke deposition resistant catalysts exhibiting stable activity [11]. Supported metals of Groups 8 (ruthenium), 9 (cobalt, rhodium, and iridium), and 10 (nickel, palladium, and platinum) were reported as potential catalysts in CDRM for their high activity in breaking C–H and C–C bonds [12,13]. The limited utilization of noble metals (Pt, Ru, Rh and Pd) due to their scarcity and high cost has increased the attention towards the studies on abundant and cheap Ni and Co based catalysts [14].

Forming a bimetallic catalyst by introducing a promoter is another appropriate option for improving the anti-coking property of CDRM catalysts, where promoters act as step-edge site blockers and/or decrease the carbon adsorption energy to prevent carbon nucleation on the catalyst [15,16].

In addition to correct selection of the catalyst components; the composition, phases and crystal structure of metal(s) and promoter(s) as well as optimized operating conditions pronouncedly enhance CDRM performance [17]. It was revealed that in high metal content catalysts larger particles, which are more prone to coke deposition through CH<sub>4</sub> decomposition on their surface, are likely to be formed [18]. Metal-support

interaction was also associated to metal loading [19]. The relation between CDRM stability, hydrogen selectivity and promoter loading, on the other hand, was confirmed with the work on Sr promoted Co/ $\gamma$ -Al<sub>2</sub>O<sub>3</sub> catalysts [20]. In another study, optimum amount of potassium (0.2 wt% K<sub>2</sub>O) was determined for very low carbon deposition and high CH<sub>4</sub> conversion in tested Ni/Al<sub>2</sub>O<sub>3</sub> catalysts [21]. The study on CeO<sub>2</sub> doped Ni/Al<sub>2</sub>O<sub>3</sub> catalysts showed that increase in Ce content results in decreasing carbon formation, but for catalysts having more than 10% Ce, lower CDRM activities due to Ni oxidation was noted [22]. Similar effect of promoter loading was observed for Ni–Mo and Co–Mo carbide catalysts: at higher molar ratios (i.e. Co/Mo above 0.4 and Ni/Mo above 0.3), phase separation of the promoter occurs causing decrease in structural and electronic promoting effects [23].

In our first paper on Co–Ce system, 5%Co–2%Ce/ZrO<sub>2</sub> catalyst was introduced as a sound alternative to PGM catalysts in CDRM. The results confirmed that this catalyst performs high CDRM activity with desired H<sub>2</sub>/CO ratio [24]. The overall purpose of the current work is to establish a link between Co/Ce loading ratio and CDRM performance of the catalyst, and to further analyze the roles of Co, Ce and ZrO<sub>2</sub> in Co–Ce/ZrO<sub>2</sub> system. To achieve this goal, catalysts with different Co and Ce loadings were prepared and their performance was tested parametrically under different temperatures and CH<sub>4</sub>/CO<sub>2</sub> feed ratios. BET, XRD, XPS, Raman and HRTEM-EDX techniques were utilized for detailed characterization. Performance and characterization results were evaluated in a combined fashion in order to shed a light to structure-activity relation for the Co–Ce/ZrO<sub>2</sub> system.

---

## Experimental

### Catalyst preparation, pretreatment and characterization

In this study, zirconia support (Alfa Aesar) was first meshed to 45–60 mesh size and then calcined at 1073 K for 4 h in muffle furnace for high thermal stability. 2%Ce/ZrO<sub>2</sub> sample was prepared via impregnation of aqueous precursor solution of Ce (cerium (III) nitrate hexahydrate, Merck). 5%Co–2%Ce/ZrO<sub>2</sub>, 5%Co–3%Ce/ZrO<sub>2</sub>, 10%Co–2%Ce/ZrO<sub>2</sub> and 10%Co–3%Ce/ZrO<sub>2</sub> catalysts were also prepared via incipient-to-wetness impregnation. After Ce impregnation, heat treatment at 773 K for 4 h in muffle furnace and impregnation of aqueous cobalt (II) nitrate hexahydrate (BDH) solution were conducted. In both impregnation steps, a Masterflex computerized-drive peristaltic pump was used to feed the precursor solution (ca. 0.6 mL/g support) to the vacuum flask at a rate of 5 mL/min via silicone tubing. The slurry in the vacuum flask was mixed by an ultrasound mixer during the impregnation in order to maintain uniform distribution of the precursor solutions. During the addition of precursor solutions, a mild vacuum was applied. After the precursor solution was added, the slurry was ultrasonically mixed for additional 90 min. The thick slurry obtained was dried at 388 K overnight at each impregnation step.

As a pretreatment, the catalysts were calcined *in situ* in dry air (30 mL/min) for 4 h at 773 K and subsequently reduced *in situ* in H<sub>2</sub> (50 mL/min) for 2 h at the same temperature based

on the preliminary tests yielding steady-state CDRM activity values. Before calcination, the temperature was risen to 773 K with 10 K/min rate under argon flow (25 mL/min). Argon flow was also introduced between calcination and reduction periods for 30 min in order to prevent the mixing of dry air and hydrogen. After reduction, argon flow was adjusted to 5 mL/min and the system was left overnight prior to the reaction tests.

The nitrogen adsorption/desorption isotherms were obtained at liquid nitrogen temperature of 77 K by using Quantachrome Nova 2200e automated gas adsorption system at Boğaziçi University Photochemistry and Photocatalysis Laboratory. The specific surface areas were determined by using multipoint BET analysis and the pores sizes were measured by the BJH method of adsorption.

The crystal structures of the Co–Ce/ZrO<sub>2</sub> and Ce/ZrO<sub>2</sub> catalyst samples and the support ZrO<sub>2</sub> were analyzed via XRD. The diffraction patterns were collected by Rigaku's D/MAX-Ultima+/PC utilizing monochromatic Cu K $\alpha$  radiation. All freshly calcined and reduced samples were continuously scanned between  $2\theta$  values of 3 and 90° with scanning speed of 0.2°/min. The measured patterns were compared with the JCPDS (Joint Committee on Powder Diffraction Standards) database for phase identification. Metal and support crystallite sizes were calculated by Scherrer equation.

The micro-structural properties of freshly calcined and reduced Co–Ce/ZrO<sub>2</sub> catalyst samples were elucidated via HRTEM, EDX and electron diffraction tests. The analyses were carried out at the Institute of Materials at TUBITAK-MAM on JEOL 2100 LaB6 HRTEM, and at METU Central Laboratory on Jem Jeol 2100F both operating at 200 kV.

The nature of interaction between the dispersed metal species and the support for fresh Co–Ce/ZrO<sub>2</sub> catalyst samples was analyzed by XPS via Thermo Scientific K-Alpha model X-ray Photoelectron Spectrometer at Boğaziçi University. All binding energies were referenced to the C1s line. For data analysis, the peak intensities were estimated by calculating the integral of each peak, after subtraction of the S-shaped Shirley-type background, and by fitting the curve to a combination of Lorentzian (30%) and Gaussian (70%) lines.

The coke deposited spent catalyst samples were analyzed by Raman spectroscopy. Raman spectra of the spent catalysts were obtained by using a Renishaw inVia Raman microscope (Advanced Technologies Research and Development Center of Boğaziçi University) with the following operation parameters: 532 nm 100 mW diode laser as the excitation source; laser intensity of ~5 mW; 10 s acquisition time; a total of 10 accumulations per spectrum. Before measurements, Raman spectrum was calibrated by using a silicon wafer peak at 520 cm<sup>-1</sup>. All the samples were analyzed under atmospheric condition without pre-treatment with the de-focusing technique.

### Catalytic performance evaluation

CDRM was carried out in a fixed-bed down-flow tubular 12 mm ID, 70 cm long quartz microreactor under atmospheric pressure. The tests were performed at the temperature interval of 873–973 K with CH<sub>4</sub>/CO<sub>2</sub> feed ratios of 1/1, 2/1, 1/2 at 20000 mL/h.g.catalyst. Hewlett Packard HP5890, temperature-

controlled and programmable gas chromatograph equipped with a Thermal Conductivity Detector and a HayeSep D analysis column, was used for analyzing feed and product gas mixtures.

## Results and discussion

### Characterization of Co–Ce/ZrO<sub>2</sub> system

Total surface area of freshly calcined and reduced ZrO<sub>2</sub> was determined as 24.41 m<sup>2</sup> g<sup>-1</sup>. As expected the BET values calculated for freshly calcined and reduced Co–Ce/ZrO<sub>2</sub> catalyst samples, slightly decreased to 22.3–23.2 m<sup>2</sup> g<sup>-1</sup> range. For all samples, the pore volumes were measured between 0.019 and 0.023 cm<sup>3</sup> g<sup>-1</sup>, and pore sizes were approximately 15 Å. The values obtained clearly indicated that ZrO<sub>2</sub> physical structure dominantly determines the characteristics of the catalyst samples; Co and Ce loadings/loading levels have no significant effect on physical characteristics.

The crystal structure of Co–Ce/ZrO<sub>2</sub> system, 2%Ce/ZrO<sub>2</sub> and ZrO<sub>2</sub> support was characterized via XRD. The spectra of all freshly calcined and reduced samples showed the presence of monoclinic zirconia (JCPDS 86-1449) (Fig. 1) with (-1 1 1) crystal plane as the most dominant phase. The intensity of m-ZrO<sub>2</sub> peaks weakened with the increase in total metal loading, due to relatively decreased ZrO<sub>2</sub> percentage, as can be seen at the inset of Fig. 1. For Co-loaded samples, peaks corresponding to (1 1 1) plane of face-centered cubic (fcc) (JCPDS 15-0806) and (1 0 1) plane of hexagonal-closed packed (hcp) (JCPDS 05-0727) structures of Co metal were also observed at  $2\theta$  values of 44.2° and 47.5°, respectively, with higher intensities for the high Co-loaded samples. Since the intensities of peaks attributed to fcc-Co(1 1 1) were higher than that of hcp-Co(1 0 1), face-centered cubic was the dominant Co metal structure in all Co-loaded samples. This phenomenon was reported widely observed among cobalt catalysts reduced at temperatures higher than 723 K [25]. Due to low ceria content and its homogeneous dispersion in all catalyst samples, peaks belonging to ceria were not detected in the XRD spectra [26].

Crystallite sizes and lattice parameters (a, b, c) were calculated for all tested samples through using the most intense reflection of the dominant structural phases, i.e. (-1 1 1) plane of m-ZrO<sub>2</sub> and (1 1 1) plane of fcc-Co, via Scherrer equation and the related lattice parameter equations. From the lattice parameters given in Table 1 for all tested samples, it can be deduced that metal addition does not lead to a major modification of crystal structures. m-ZrO<sub>2</sub> crystallite sizes were calculated around 21 nm for all samples. Co metal crystallite sizes, on the other hand, were lower for 10% Co loaded catalysts and increased with the increase in Ce content due to crystal defects and/or dislocations.

It was also noticed that the peaks in the spectrum of 10% Co–2%Ce/ZrO<sub>2</sub> catalyst shifted to lower  $2\theta$  values indicating expansion of interplanar spacing [27] as also shown with d-spacing values in Table 1. This might be attributed to lattice mismatching and/or distortion [28] due to more lattice oxygen vacancies in this sample [29].

Micro-structural properties of Co–Ce/ZrO<sub>2</sub> system and dispersion of Co and Ce on catalyst samples were analyzed by

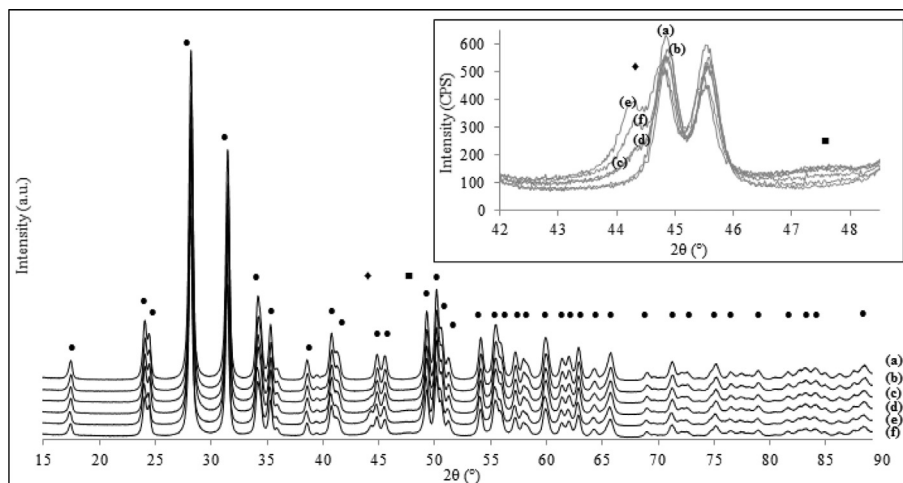


Fig. 1 – XRD patterns for freshly calcined and reduced (a)  $\text{ZrO}_2$ , (b) 2%Ce/ $\text{ZrO}_2$ , (c) 5%Co–2%Ce/ $\text{ZrO}_2$ , (d) 5%Co–3%Ce/ $\text{ZrO}_2$ , (e) 10%Co–2%Ce/ $\text{ZrO}_2$  and (f) 10%Co–3%Ce/ $\text{ZrO}_2$  samples. (●: m- $\text{ZrO}_2$ , ◆: fcc-Co metal, ■: hcp-Co metal).

Table 1 – d-spacing values and calculated lattice parameters and crystallite sizes for the tested samples. (n.d. = “not determined”).

Sample	$d_{\text{m-ZrO}_2}$ (Å)	$d_{\text{fcc-Co}}$ (Å)	$d_{\text{hcp-Co}}$ (Å)	m- $\text{ZrO}_2$ crystallite size (nm)	fcc-Co crystallite size (nm)	Lattice parameters for the support (Å)			Lattice parameters for fcc-Co (Å)
						a	b	c	a
$\text{ZrO}_2$	3.16	n.d.	n.d.	21.44	n.d.	5.11	5.21	5.31	
2%Ce/ $\text{ZrO}_2$	3.16	n.d.	n.d.	21.40	n.d.	5.10	5.20	5.30	
5%Co–2%Ce/ $\text{ZrO}_2$	3.16	2.04	3.54	21.61	34.31	5.11	5.21	5.31	3.54
5%Co–3%Ce/ $\text{ZrO}_2$	3.16	2.04	3.54	21.28	38.64	5.11	5.21	5.31	3.54
10%Co–2%Ce/ $\text{ZrO}_2$	3.17	2.04	3.54	21.05	13.42	5.12	5.22	5.32	3.54
10%Co–3%Ce/ $\text{ZrO}_2$	3.16	2.04	3.54	20.95	14.29	5.11	5.21	5.31	3.54

HRTEM and EDX. The existence of Co, Ce and  $\text{ZrO}_2$  particles were verified via EDX analysis given in Fig. 2. The HRTEM images in the same figure also expressed that local  $\text{ZrO}_2$  particles size is 2–5 times higher than that of Co and Ce.

The nanobeam diffraction analysis applied to HRTEM images for 5%Co–2%Ce/ $\text{ZrO}_2$  catalyst sample (Fig. 3a) gave d-spacing values corresponding to monoclinic zirconia of (1 1 0) and (0 2 2) planes. In another region of the same sample, d-spacing value for CoO in (1 1 1) plane was detected in addition to that of monoclinic zirconia of (1 1 0) plane (Fig. 3b).

The comparison of HRTEM area images in Fig. 4 for 5%Co–2%Ce/ $\text{ZrO}_2$ , 10%Co–2%Ce/ $\text{ZrO}_2$  and 10%Co–3%Ce/ $\text{ZrO}_2$  revealed that in general Co/Ce ratio does not impose significant micro-physical changes on catalyst surface.

The mapping results obtained in this study verified our previous findings [24] by showing nonhomogeneous dispersion of Co particles and even distribution of Ce particles (Fig. 5). The EDX-Line analysis utilized for another region of the 5%Co–2%Ce/ $\text{ZrO}_2$  catalyst sample also highlighted that Ce particles are well dispersed but low in amount; whereas Co particles are found as clusters (Fig. 6). This phenomenon was also valid for the other tested catalyst samples. According to HRTEM-EDX results, for example, Co/Ce ratio values ranged in between 0.18 and 2.63 (wt%/wt%) for 10%Co–3%Ce/ $\text{ZrO}_2$

catalyst. It might be suggested that Co particles partially cover Ce particles during its impregnation; as an example, similar phenomenon was observed in the work of Miyazawa et al. where some of the Co particles were covered by Mn and Zr particles during sequential impregnation [30].

In order to analyze the redox ability of  $\text{CeO}_x$  formations and how it is affected by Co/Ce ratio, Ce3d XPS spectra of the freshly reduced and spent Co–Ce/ $\text{ZrO}_2$  catalyst samples were obtained (Fig. 7). Overall surface Ce%, on atomic basis, was calculated as 13.2, 17.8, 9.6 and 16.3 for 5%Co–2%Ce/ $\text{ZrO}_2$ , 5%Co–3%Ce/ $\text{ZrO}_2$ , 10%Co–2%Ce/ $\text{ZrO}_2$ , and 10%Co–3%Ce/ $\text{ZrO}_2$  catalysts, respectively. For 10%Co–2%Ce/ $\text{ZrO}_2$ , this explained the lower intensity values, which were expected because of the highest Co/Ce ratio (Fig. 7). In literature, three main  $3d_{5/2}$  peaks at about 882.5 (v), 888.8 (v<sup>2</sup>) and 898.3 (v<sup>3</sup>) eV and three main  $3d_{3/2}$  peaks at about 901 (u), 907.4 (u<sup>2</sup>) and 916.6 (u<sup>3</sup>) eV, belonging to  $\text{Ce}^{4+}$  state were reported, while the peaks at about 880.5 (v<sub>0</sub>), 885.4 (v<sup>1</sup>), 898.8 (u<sub>0</sub>) and 904 (u<sup>1</sup>) eV were matched to  $\text{Ce}^{3+}$  state [31]. The binding energies attributed to  $\text{Ce}^{4+}$  and  $\text{Ce}^{3+}$  states, given in Table 2, were found in accordance with literature for all catalyst samples; as there was no shift in the binding energies of the Ce peaks compared to those of the literature, the results pointed out that for the catalyst samples tested, even surface alloy formation is of small probability.



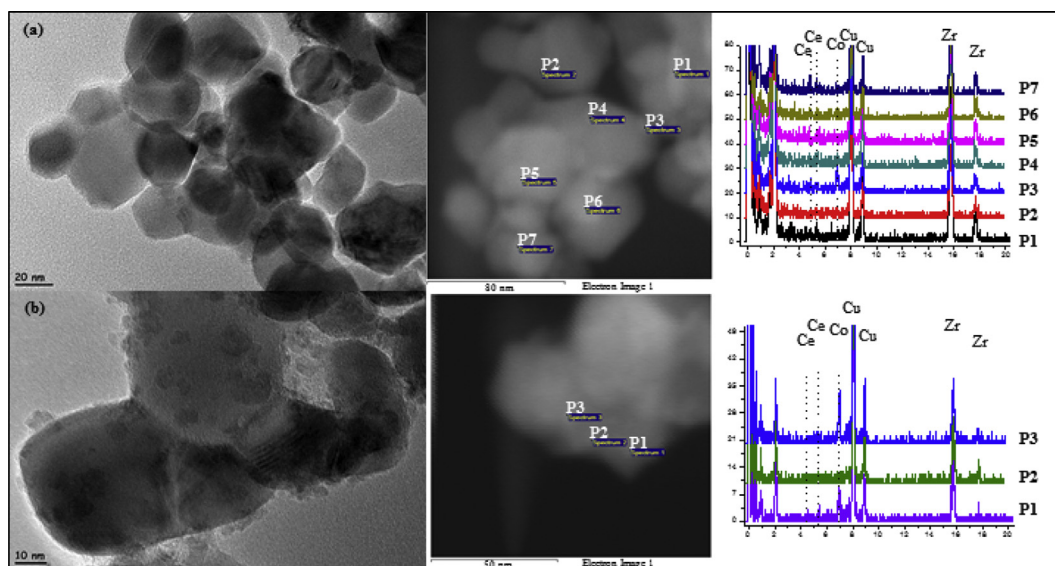


Fig. 2 – HRTEM area images and EDX results for freshly calcined and reduced (a) 5%Co–2%Ce/ZrO<sub>2</sub>, and (b) 10%Co–3%Ce/ZrO<sub>2</sub> catalysts.

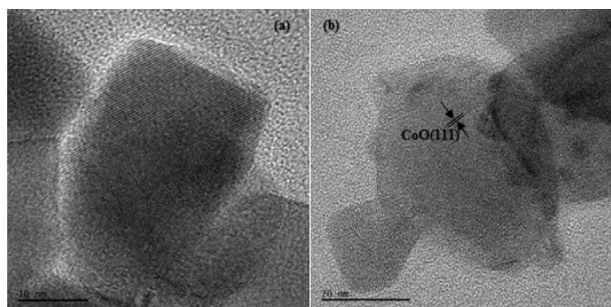


Fig. 3 – HRTEM images of freshly calcined and reduced 5%Co–2%Ce/ZrO<sub>2</sub> catalyst.

The degree of ceria reduction was evaluated after deconvolution of each spectrum by taking the ratio of the sum of integrated areas of  $v_0$ ,  $u_0$ ,  $u^1$  and  $v^1$  peaks to the sum of the integrated peak areas of all peaks, as given in Equation (1):

$$[\text{Ce}^{3+}] = \frac{I - \text{Ce}^{3+}}{I - \text{Ce}^{3+} + I - \text{Ce}^{4+}} \quad (1)$$

where  $I - \text{Ce}^{3+}$  and  $I - \text{Ce}^{4+}$  represent the sum of intensities of two doublets resulting from Ce<sub>2</sub>O<sub>3</sub> and three doublets resulting from CeO<sub>2</sub>, respectively [31]. It was argued that higher degree of ceria reduction leads to an increase in the mobility of oxygen ions [32]. The deconvolution analysis established the degrees of ceria reduction as 27.8, 26.5, 22.1 and 27.7% for the 5%Co–2%Ce/ZrO<sub>2</sub>, 5%Co–3%Ce/ZrO<sub>2</sub>, 10%Co–2%Ce/ZrO<sub>2</sub>, and 10%Co–3%Ce/ZrO<sub>2</sub> catalysts, respectively. The lowest degree of ceria reduction estimated for 10%Co–2%Ce/ZrO<sub>2</sub> might be explained by its highest Co/Co ratio. Therefore, it is suggested that not only Ce amount but also the Co/Co ratio should play a role in CDRM performance -and perhaps CDRM kinetics- of the Co–Ce catalysts.

To obtain information about support defects on catalysts, O1s spectra was utilized (Fig. 8). Accordingly, the peak at 528–530 eV corresponds to lattice oxygen of CeO<sub>2</sub>, ZrO<sub>2</sub> and CoO phases [33–36], whereas peaks at 531–533 eV belong to adsorbed oxygen and lattice oxygen vacancies, which are formed as a result of highly polarized oxygen atoms at the surface and interphase of low coordination numbered nanocrystallites [34,37,38]. Blue shift of the spectrum for 10%Co–2%Ce/ZrO<sub>2</sub> can be attributed to doping effect on support [38]. Since

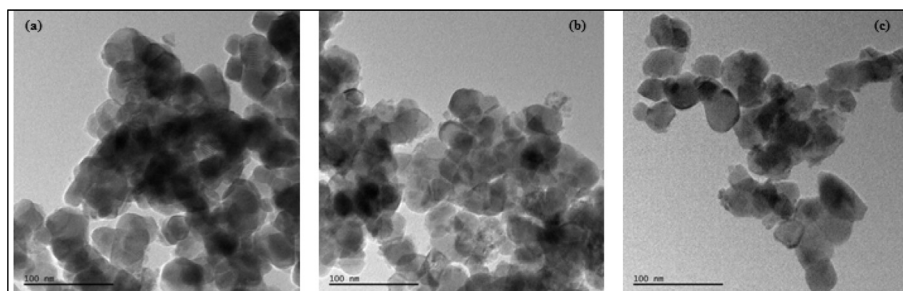


Fig. 4 – HRTEM area images for freshly calcined and reduced (a) 5%Co–2%Ce/ZrO<sub>2</sub>, (b) 10%Co–2%Ce/ZrO<sub>2</sub>, and (c) 10%Co–3%Ce/ZrO<sub>2</sub> catalysts.

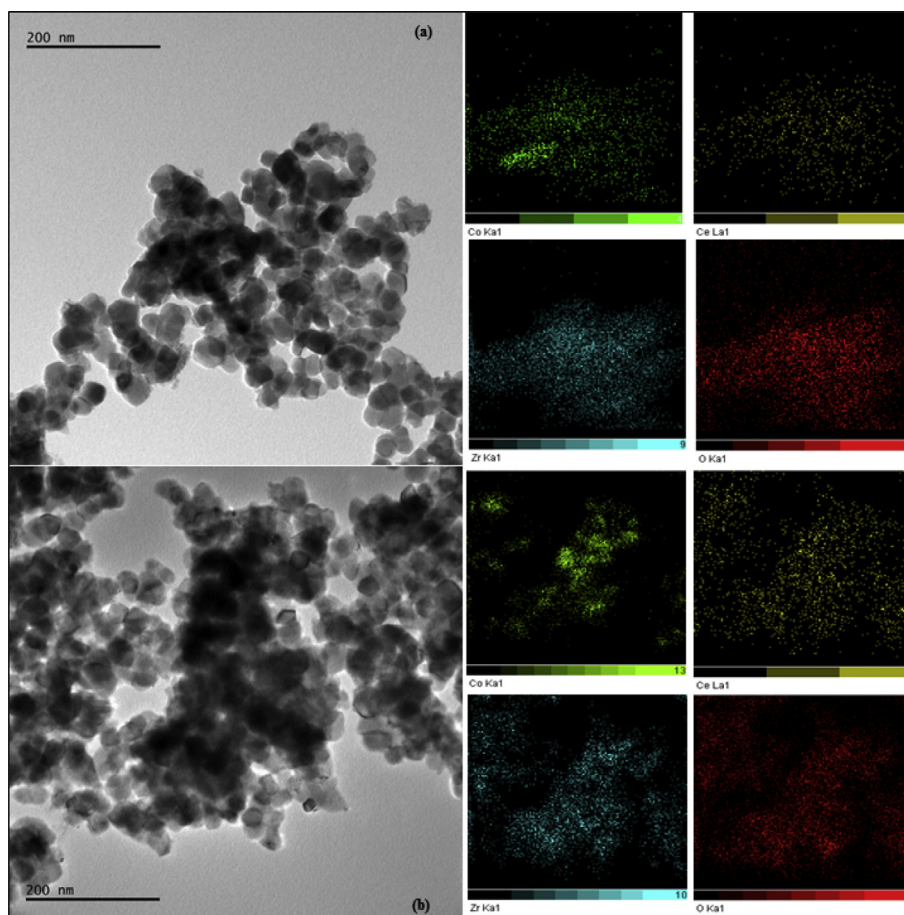


Fig. 5 – HRTEM image and Co, Ce, Zr and O mapping of the related region for freshly calcined and reduced (a) 5%Co–2%Ce/ZrO<sub>2</sub> and (b) 10%Co–3%Ce/ZrO<sub>2</sub> catalysts.

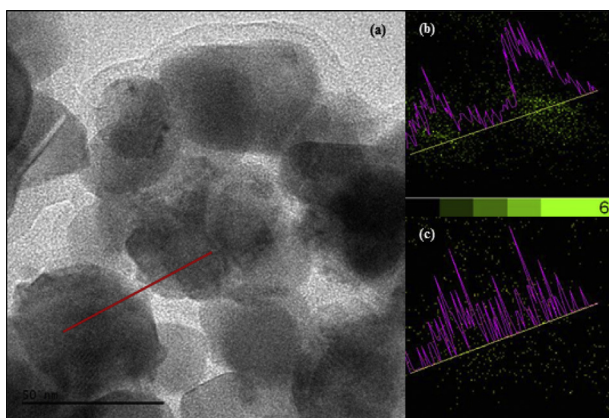


Fig. 6 – (a) HRTEM image of freshly calcined and reduced 5% Co–2%Ce/ZrO<sub>2</sub> catalyst, (b) Co EDX-Line and mapping analysis, (c) Ce EDX-Line and mapping analysis of the selected region. (Selected region is indicated by a line in (a)).

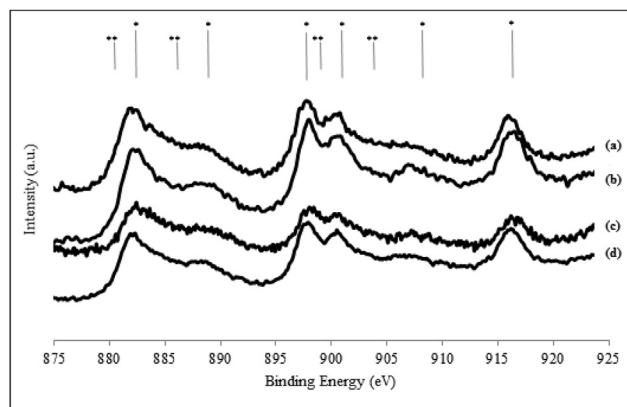


Fig. 7 – XP spectra of Ce3d region for freshly calcined and reduced (a) 5%Co–2%Ce/ZrO<sub>2</sub>, (b) 5%Co–3%Ce/ZrO<sub>2</sub>, (c) 10%Co–2%Ce/ZrO<sub>2</sub>, and (d) 10%Co–3%Ce/ZrO<sub>2</sub> (\*: Ce<sup>4+</sup>, \*\*: Ce<sup>3+</sup>).

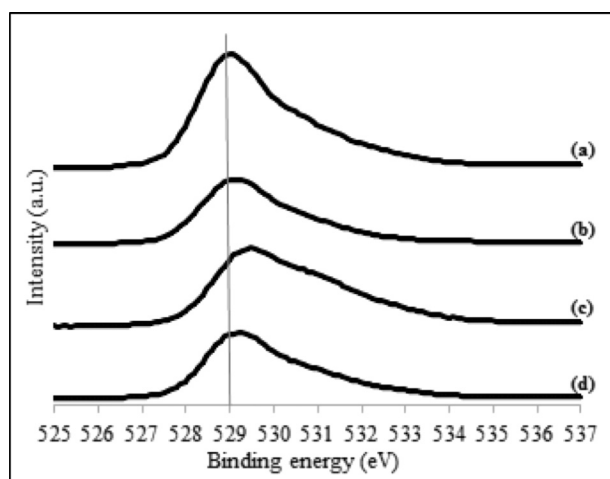
the lowest intensity values were already observed at Ce3d spectrum for this catalyst (Fig. 7), this might hint that cerium atoms are incorporated in zirconia lattice which causes oxygen vacancies [38]. Additionally, the highest asymmetry of the spectrum was observed for this catalyst due to lattice oxygen

vacancies and adsorbed oxygen [34]. This outcome validates the above mentioned XRD results which hinted higher amount of oxygen defects in 10%Co–2%Ce/ZrO<sub>2</sub> sample.

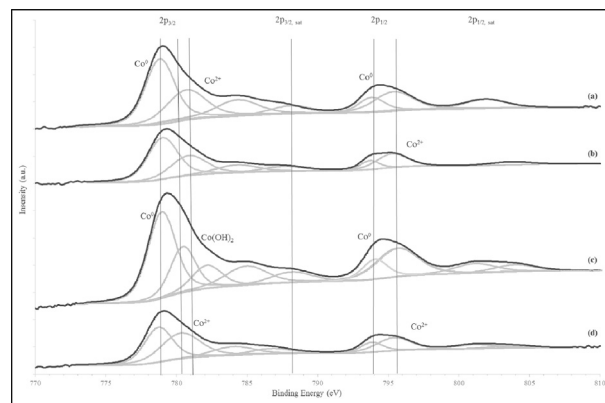
Differentiation of cobalt species having different oxidation states and correlation of their (relative) amounts to catalytic

**Table 2 – The Ce valance-binding energy (eV) relation for different freshly calcined and reduced catalyst samples.**

Catalyst	Ce Valance	Binding energy, eV
5%Co–2%Ce/ZrO <sub>2</sub> [18]	Ce <sup>4+</sup>	916.06, 907.22, 900.56, 897.54, 888.57, 882.5
	Ce <sup>3+</sup>	903.47, 898.92, 884.85, 879.36
	Ce <sup>4+</sup>	916.75, 907.7, 901.07, 898.29, 889.37, 882.68
5%Co–3%Ce/ZrO <sub>2</sub>	Ce <sup>4+</sup>	916.75, 907.7, 901.07, 898.29, 889.37, 882.68
	Ce <sup>3+</sup>	903.43, 898.65, 885.72, 880.63
10%Co–2%Ce/ZrO <sub>2</sub>	Ce <sup>4+</sup>	916.39, 907.76, 900.85, 897.79, 889.1, 882.4
	Ce <sup>3+</sup>	904.13, 899.44, 885.43, 879.56,
10%Co–3%Ce/ZrO <sub>2</sub>	Ce <sup>4+</sup>	916.15, 906.96, 900.54, 897.62, 888.46, 881.88
	Ce <sup>3+</sup>	902.69, 899.09, 884.54, 879.77

**Fig. 8 – XP spectra of O1s region for freshly calcined and reduced (a) 5%Co–2%Ce/ZrO<sub>2</sub>, (b) 5%Co–3%Ce/ZrO<sub>2</sub>, (c) 10%Co–2%Ce/ZrO<sub>2</sub>, and (d) 10%Co–3%Ce/ZrO<sub>2</sub>.**

properties, especially when they are in interaction with support, is known to be a challenging task [39]. The XP spectra of Co2p region, given in Fig. 9 for all catalyst samples, were analyzed in detail. The peaks at 778.8 and 793.7 eV, separated by 14.9 eV, which were reported as Co2p<sub>3/2</sub> and Co2p<sub>1/2</sub> peaks, respectively, of Co<sup>0</sup> phase in literature [39,40], indicate the metallic nature of catalyst surface. Surface metallic Co concentrations were calculated as 41.1, 44.1, 37.0 and 35.0% for 5% Co–2%Ce/ZrO<sub>2</sub>, 5%Co–3%Ce/ZrO<sub>2</sub>, 10%Co–2%Ce/ZrO<sub>2</sub>, and 10%Co–3%Ce/ZrO<sub>2</sub> catalysts, respectively, highlighting the possibility of metal oxidation for catalysts having higher Co loading. Co oxide phases are reported as hard to distinguish due to the small shifts in their binding energy values [41,42]. The Co2p<sub>3/2</sub> peak at 780–781 eV corresponds to oxide states of Co [43,44] and the peak with no satellite was stated as a signature of Co<sup>3+</sup> phase [45]. On the other hand, the peak with an intense satellite at a distance of 6 eV was attributed to Co<sup>2+</sup>

**Fig. 9 – XP spectra of Co2p region for freshly calcined and reduced (a) 5%Co–2%Ce/ZrO<sub>2</sub>, (b) 5%Co–3%Ce/ZrO<sub>2</sub>, (c) 10%Co–2%Ce/ZrO<sub>2</sub>, and (d) 10%Co–3%Ce/ZrO<sub>2</sub>.**

phase in CoO [39,46]. As can be clearly seen from Fig. 9, Co<sup>2+</sup> peaks with their satellite features for CoO are present in spectra of all catalysts. HRTEM analysis (Fig. 3b) has also verified the existence of CoO. The red shift of Co<sup>2+</sup> peak positions from 781 to 780.4 eV for the catalysts with higher Co loading verifies that Co species in these samples are more oxidized [47]. It should be noted that the peak at 782.5 eV, which is only observed for 10%Co–2%Ce/ZrO<sub>2</sub>, is attributed to Co(OH)<sub>2</sub> and Co<sub>3</sub>O<sub>4</sub> [42,48] which contain both Co<sup>3+</sup> and Co<sup>2+</sup> species.

#### CDRM performance of Co–Ce/ZrO<sub>2</sub> system

Aiming to investigate the roles of each species and to observe the effects of Co and Ce loading and Co/Ce ratio on CDRM performance of Co–Ce/ZrO<sub>2</sub> system, 5%Co–2%Ce/ZrO<sub>2</sub>, 5%Co–3%Ce/ZrO<sub>2</sub>, 10%Co–2%Ce/ZrO<sub>2</sub> and 10%Co–3%Ce/ZrO<sub>2</sub> were parametrically tested for their CDRM activity and selectivity at different temperatures (873 K, 923 K and 973 K) and CH<sub>4</sub>/CO<sub>2</sub> feed ratios (1/1, 1/2 and 2/1) at fixed space velocity, 20000 mL/h.g.catalyst. In this context, CH<sub>4</sub> and CO<sub>2</sub> conversion, activity, H<sub>2</sub> yield and selectivity were obtained for all the above mentioned samples. H<sub>2</sub>/CO product ratio was considered as a measure of selectivity. The activity values were calculated according to the given equation (Equation (2)):

$$\text{CH}_4 \text{ or CO}_2 \text{ Activity} = (\text{CH}_4 \text{ or CO}_2 \text{ Flow Rate in Feed Stream} - \text{CH}_4 \text{ or CO}_2 \text{ Flow Rate in Product Stream}) / \text{Catalyst Weight} \quad (2)$$

6 h time-on-stream (TOS) data obtained over the catalysts in the performance tests conducted at 973 K with 1/1 CH<sub>4</sub>/CO<sub>2</sub> feed ratio (Fig. 10) showed that the highest CH<sub>4</sub> and CO<sub>2</sub> activity values, 76 and 89 μmol/s.g.catalyst, respectively, were recorded for the catalyst with 10% Co and 2% Ce loading. High activity values were also noted for 10%Co–3%Ce/ZrO<sub>2</sub> catalyst. However, the tests conducted over these catalysts resulted in more carbon deposition than the ones over 5% Co-loaded samples. Increased carbon deposition yielded higher CH<sub>4</sub> activity loss values as well; the percentage activity losses



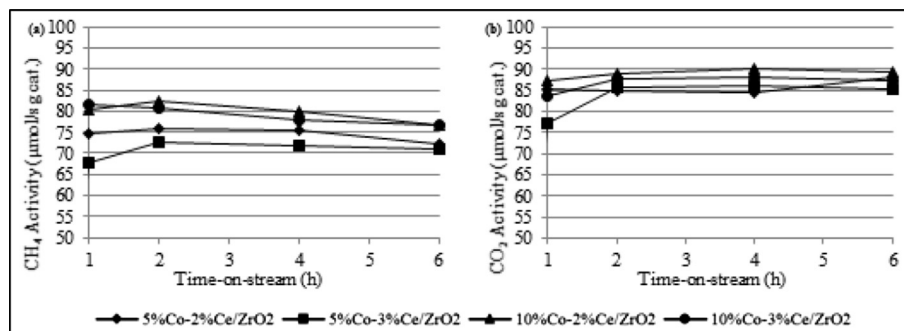


Fig. 10 – Activity profiles of tested catalysts at 973 K with 1/1  $\text{CH}_4/\text{CO}_2$  feed ratio (a)  $\text{CH}_4$  activity, and (b)  $\text{CO}_2$  activity.

at the end of 6 h TOS were calculated as 7% and 5% for 10%Co–2%Ce/ZrO<sub>2</sub> and 10%Co–3%Ce/ZrO<sub>2</sub>, respectively. This points out that Co is mainly related to  $\text{CH}_4$  dehydrogenation activity [24], and that there is not enough surface oxygen to clean away carbon formed by  $\text{CH}_4$  dehydrogenation due to relatively low amount of Ce and ZrO<sub>2</sub> for high Co loaded samples. Therefore, it can indirectly be seen that both Ce and ZrO<sub>2</sub> have roles in surface oxygen production/transfer. It should be noted that the reason for low surface Ce concentration of high Co-loaded samples is explained by Co formations covering Ce sites during catalyst preparation. The lack of Co–Ce synergistic interaction, weakening oxygen storage and transfer between species, should also be noted for the catalysts with higher Co/Ce ratio. Moreover, catalysts with 10% Co loading were found to contain more oxidized Co species according to Co2p XPS results which may lead to catalyst deactivation due to metal sintering [49–52], since surface oxidized medium assists particle migration, coalescence and collision [53]. On the other hand, low activity values observed in the performance tests over 5%Co–3%Ce/ZrO<sub>2</sub> catalyst for the first 2 h TOS can be explained by the relatively lower  $\text{CH}_4$  dehydrogenation activity compared to that of  $\text{CO}_2$  dissociation, which also strengthened the idea that Co is primarily effective in  $\text{CH}_4$  dehydrogenation. The unaffected  $\text{CO}_2$  activation indicated that ZrO<sub>2</sub> is responsible for surface oxygen production by  $\text{CO}_2$  dissociation; since the support of this catalyst is less covered by metals compared to those with 10% Co loading. Therefore, ceria's role is mainly the transfer of this surface oxygen by creating a continuous oxidation/reduction cycle to keep the metal surface free of carbon [11]. Relatively limited  $\text{CO}_2$  activity decrease compared to that of  $\text{CH}_4$  also supports that explanation.

When the selectivity profiles of all catalysts were compared for the tests conducted at 973 K with 1/1  $\text{CH}_4/\text{CO}_2$  feed ratio (Fig. 11), it was seen that the catalyst with 10% Co and 2% Ce loading gave the highest  $\text{H}_2/\text{CO}$  ratio throughout 6 h TOS. However, the values decreased sharply and stable product ratio could not be obtained for that sample. This might be due to the closure of active sites responsible for  $\text{H}_2$  production by deposited carbon from methane decomposition [1,24]. Same trend was also observed for the tests conducted over 10%Co–3%Ce/ZrO<sub>2</sub> and 5%Co–3%Ce/ZrO<sub>2</sub> catalysts. On the other hand, the catalyst with 5% Co and 2% Ce loading gave the most stable selectivity profile, which can be

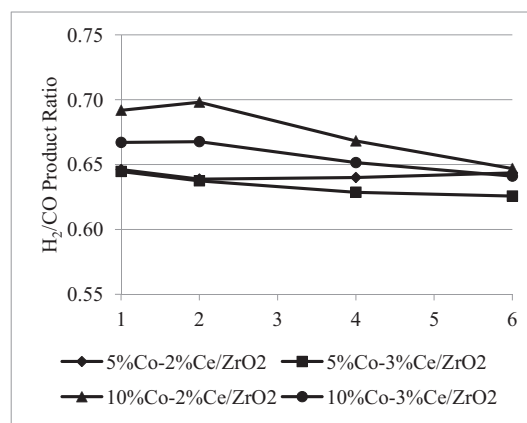


Fig. 11 – Selectivity profiles of tested catalysts at 973 K with 1/1  $\text{CH}_4/\text{CO}_2$  feed ratio.

explained through the balance between C-formation and C-oxidation led by enhanced mobility of surface oxygen, verified by XPS analysis.

Since CDRM contains many side reactions favored at different temperature levels, changing the temperature affects the performance of catalysts. Carbon forming reactions – Boudouard reaction and methane decomposition – and oxygen producing reaction – dissociative adsorption of  $\text{CO}_2$  – are the most important reactions affecting the CDRM performance; dissociative  $\text{CO}_2$  adsorption needs to be at least as fast as the former ones in order to prevent coke deposition. Boudouard reaction is an exothermic reaction favored at low temperatures, whereas methane decomposition is favored at high temperatures [3]. Considering these trends, performance tests were applied by keeping the feed ratio as 1/1 but decreasing the CDRM temperature in order to grasp the performance characteristics in 873–973 K range. For all tested catalysts, both  $\text{CH}_4$  and  $\text{CO}_2$  activity values and  $\text{H}_2/\text{CO}$  ratios decreased with the decrease in temperature (Figs. 12 and 13). The lower activity values can be explained with the endothermic nature of CDRM [1] whereas the trend in selectivity values are related to favored RWGS at low temperatures [54]. The activity order of the tested catalysts also changed with the decrease in temperature, pointing out the effect of metal and promoter content in rates of side reactions.

At 923 K, 10%Co–2%Ce/ZrO<sub>2</sub>, the catalyst with the highest Co/Ce ratio, showed a very unstable  $\text{CH}_4$  activity, which might



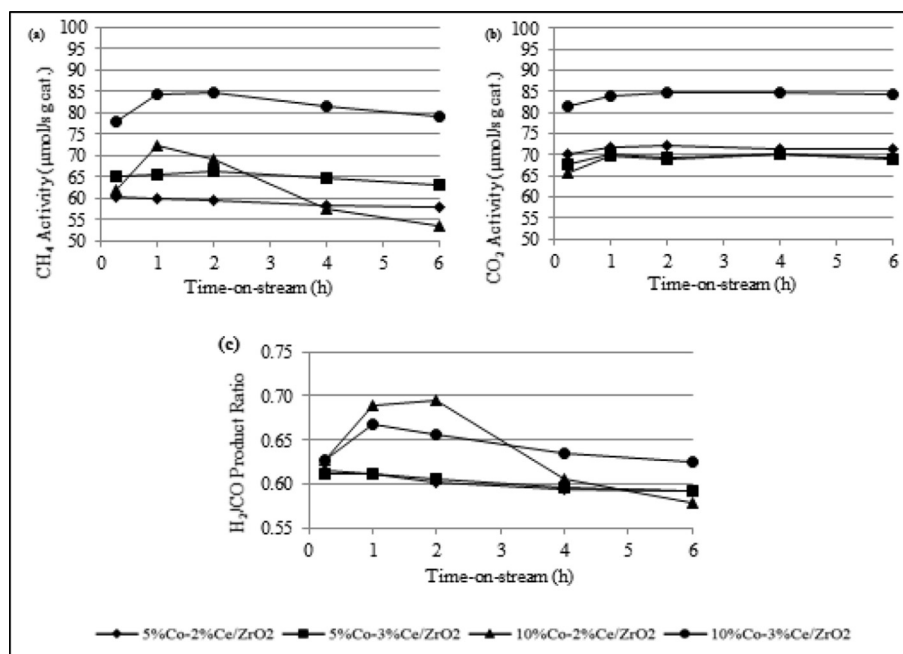


Fig. 12 – Activity and selectivity profiles of tested catalysts at 923 K with 1/1 CH<sub>4</sub>/CO<sub>2</sub> feed ratio (a) CH<sub>4</sub> activity, (b) CO<sub>2</sub> activity, and (c) H<sub>2</sub>/CO product ratio.

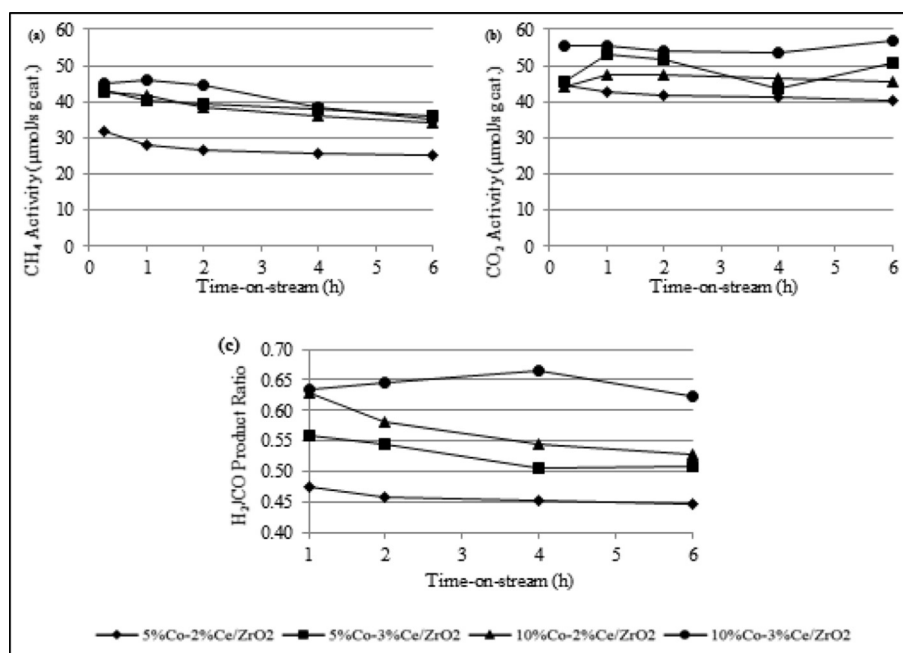


Fig. 13 – Activity and selectivity profiles of tested catalysts at 873 K with 1/1 CH<sub>4</sub>/CO<sub>2</sub> feed ratio (a) CH<sub>4</sub> activity, (b) CO<sub>2</sub> activity, and (c) H<sub>2</sub>/CO product ratio.

be related to its high Co loading, and therefore, favored CH<sub>4</sub> decomposition which caused coke accumulation (Fig. 12). The highest CH<sub>4</sub> and CO<sub>2</sub> activity values and H<sub>2</sub>/CO ratio, on the other hand, were obtained over 10%Co-3%Ce/ZrO<sub>2</sub> catalyst underlining the positive effect of both Ce and Ce<sup>3+</sup> on both CDRM activity and selectivity. Ce limits the activity loss

related to coke deposition. Additionally, the selectivity values for the catalysts with 10% Co loading varied a lot as the reaction proceeded proving that the rate of carbon removal was less than that of carbon formation. More stable activity and selectivity profiles were obtained for the catalysts with 5% Co loading. It was also interesting to note that the effect of Ce on

both activity and selectivity was less noticeable for the catalysts with 5% Co loading. This might hint that Ce is less utilized when there are more reduced Co species, since surface  $\text{Co}^0$  concentrations were recorded as highest for 5% Co loaded catalysts in XPS analysis.

When the temperature was further decreased to 873 K (Fig. 13), the highest  $\text{CH}_4$  and  $\text{CO}_2$  activity values were recorded for 5%Co–3%Ce/ $\text{ZrO}_2$  and 10%Co–3%Ce/ $\text{ZrO}_2$ , respectively, at 6 h TOS. This difference most probably stemmed from the relative change in the rates of  $\text{CO}_2$  dissociation and  $\text{CH}_4$  decomposition. It should also be noted that CDRM activities of the catalysts with 10% Co loading decreased more with decline in temperature, compared to other catalysts; confirming the role of Co on  $\text{CH}_4$  decomposition which is less favored at low temperatures. At 6 h TOS, 21% loss in  $\text{CH}_4$  activity values was calculated for 10%Co–3%Ce/ $\text{ZrO}_2$ , which might result from carbon accumulation. High activity losses, also observed at 10%Co–2%Ce/ $\text{ZrO}_2$  and 5%Co–3%Ce/ $\text{ZrO}_2$  catalysts, yield to a stability problem that stands as an obstacle for the industrial use of these catalysts. 5%Co–2%Ce/ $\text{ZrO}_2$  catalyst, on the other hand, showed a very stable profile even for 72 h TOS as indicated in our previous study [24].

From the parametric temperature analysis, it might also be concluded that carbon is deposited at sites that are active in  $\text{CH}_4$  dehydrogenation [24], since  $\text{CH}_4$  activity loss was faster than that of  $\text{CO}_2$ , especially for the catalysts with 10% Co loading.

$\text{CH}_4/\text{CO}_2$  feeding ratio is another important CDRM parameter as  $\text{CO}_2$  acts as the oxygen source whereas excess  $\text{CH}_4$  favors carbon formation. In addition to the performance tests with  $\text{CH}_4/\text{CO}_2 = 1/1$ , tests at two other feed ratios, 1/2 and 2/1, were conducted to analyze how the effect of Co/Ce loading on CDRM performance was enhanced or suppressed by feed

composition. It should be noted that as reactant flow rates would be different for each  $\text{CH}_4/\text{CO}_2$  feed ratio, conversion values, through which the results with different reactant flow rates can be compared, are used for discussion.

Increasing  $\text{CH}_4$  source in the feed, i.e. using  $\text{CH}_4/\text{CO}_2 = 2/1$ , mainly caused stability problem through coke deposition, especially during first 2 h of the reaction for all temperature levels. For example, the activity loss in terms of  $\text{CH}_4$  conversion was recorded as 41% for the test conducted over 10%Co–2%Ce/ $\text{ZrO}_2$  at 973 K (Fig. 14a). The lowest activity loss at this temperature was noted as 19% over 5%Co–2%Ce/ $\text{ZrO}_2$ . As 5%Co–2%Ce/ $\text{ZrO}_2$  and 10%Co–2%Ce/ $\text{ZrO}_2$  are the catalysts having the highest and lowest  $\text{Ce}^{3+}$  concentrations, respectively, and as the highest deactivation was observed for 10% Co loaded catalysts, which have higher concentration of oxidized Co species; the combined evaluation of characterization and performance tests results revealed that Co/Ce ratio plays a plausible role in CDRM mechanism. This can be explained by Co/Ce ratio impact on reaction environment (oxidative or reductive) which favors the regeneration of metallic Co and the  $\text{CH}_4$  dehydrogenation reaction when it is reductive, while yields the oxidation of metallic Co sites when oxidative [51,52].

On the other hand, the increase in the feeding rate of  $\text{CO}_2$ , i.e. using  $\text{CH}_4/\text{CO}_2 = 1/2$ , created a noticeable decrease in the activity losses in terms of both  $\text{CH}_4$  and  $\text{CO}_2$  conversions at 2 h TOS. This might have occurred because when the feed was rich in oxygen source, surface oxygen formation and its effective transfer to Co sites – via  $\text{CO}_2$  dissociation on  $\text{ZrO}_2$  forming surface oxygen followed by transfer of surface oxygen to Co sites regulated by Ce-prevented coke accumulation. At 973 K, where  $\text{CH}_4$  dehydrogenation was mostly favored, the combined effect of  $\text{ZrO}_2$  and Ce can be more clearly observed



Fig. 14 – Activity profiles in terms of  $\text{CH}_4$  conversion for tested catalysts at 973 K (a) with the feed ratio of 2/1 (b) with the feed ratio of 1/2, and (c) for all tested feed ratios.

(Fig. 14b); CH<sub>4</sub> conversion dropped only by 3% for the test conducted on the catalyst with the lowest Co/Ce ratio and relatively high ZrO<sub>2</sub> content, i.e. 5%Co–3%Ce/ZrO<sub>2</sub>. The percentage activity loss increased with the increase in Co/Ce ratio and became 10% for the catalyst with the highest Co/Ce ratio, i.e. 10%Co–2%Ce/ZrO<sub>2</sub>.

At the feed ratio of CH<sub>4</sub>/CO<sub>2</sub> = 2/1, suffering from lack of surface oxygen to clean away formed carbon on active sites also led to lower conversion values, in terms of both CH<sub>4</sub> and CO<sub>2</sub>, compared to those recorded for the other feed ratios (Fig. 14c). The effect of favored RWGS at CO<sub>2</sub>-rich environment might also be considered, since its by-product H<sub>2</sub>O enhances methane steam reforming as a side reaction yielding higher methane conversion values at the feed ratio of CH<sub>4</sub>/CO<sub>2</sub> = 1/2 [1]. Conversion values at the end of 6 h TOS, on the other hand, were close to each other for all tested catalysts at each temperature level. At 973 K, for example, 6 h TOS CH<sub>4</sub> conversion values were 34.1%, 33.3%, 34.9% and 35.2% for 5%Co–2%Ce/ZrO<sub>2</sub>, 10%Co–2%Ce/ZrO<sub>2</sub>, 5%Co–3%Ce/ZrO<sub>2</sub> and 10%Co–3%Ce/ZrO<sub>2</sub>, respectively. At CH<sub>4</sub>/CO<sub>2</sub> feed ratio of 1/2, the highest conversion values were recorded for the catalysts with 10% Co loading at all temperature levels showing that increased oxygen source in the feed can overcome the rapid coke formation that would be led by high CH<sub>4</sub> dehydrogenation activity of the catalysts having high Co loading.

For the tests conducted at CH<sub>4</sub>/CO<sub>2</sub> feeding ratio of 2/1, it was also clearly noticed that the catalysts with the same cobalt loading displayed exactly the same selectivity profiles at all temperatures (Fig. 15). Therefore, it can be said that at CH<sub>4</sub>/CO<sub>2</sub> feed ratio of 2/1, CH<sub>4</sub> dehydrogenation performance plays the major role in determining the selectivity. It can additionally be concluded that Ce has limited effect on selectivity when there is not enough surface oxygen, underlining that Ce is only responsible for oxygen transfer but not its formation. When CO<sub>2</sub> concentration in the feed was increased (figure not shown), H<sub>2</sub>/CO ratio values were converged to ca. 0.52 at the

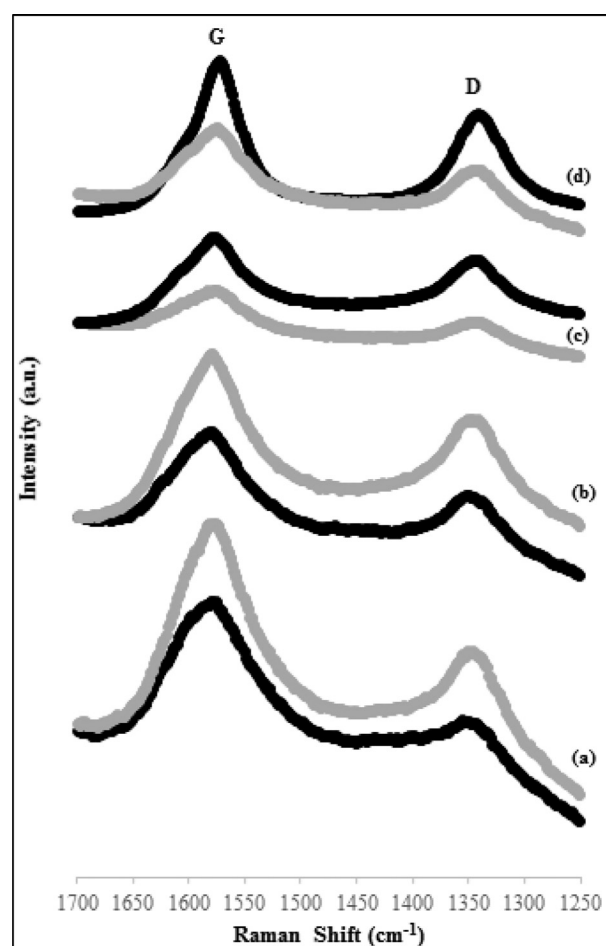


Fig. 16 – Raman spectra of (a) 5%Co–2%Ce/ZrO<sub>2</sub>, (b) 5%Co–3%Ce/ZrO<sub>2</sub>, (c) 10%Co–2%Ce/ZrO<sub>2</sub> and (d) 10%Co–3%Ce/ZrO<sub>2</sub> used during the reaction at 973 K, CH<sub>4</sub>/CO<sub>2</sub> = 2/1 (black curve); 873 K, CH<sub>4</sub>/CO<sub>2</sub> = 1/1 (grey curve).

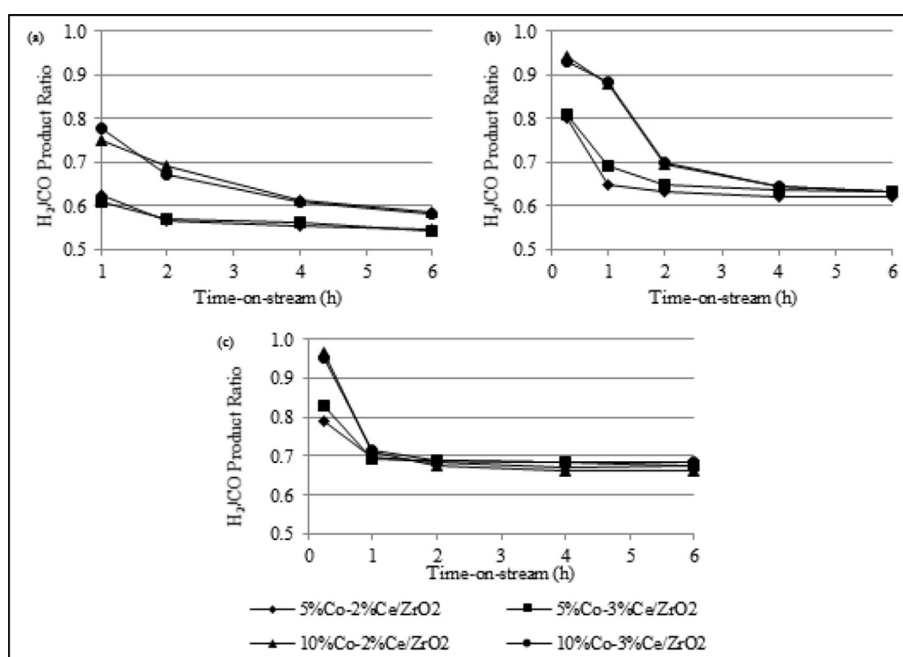


Fig. 15 – Selectivity profiles of tested catalysts with the feed ratio of 2/1 at (a) 873 K, (b) 923 K and (c) 973 K.



**Table 3 – Raman analysis results for all samples tested at different conditions.**

Catalyst	873 K, CH <sub>4</sub> /CO <sub>2</sub> = 1/1			973 K, CH <sub>4</sub> /CO <sub>2</sub> = 2/1		
	Raman shift of D band (cm <sup>-1</sup> )	Raman shift of G band (cm <sup>-1</sup> )	I <sub>D</sub> /I <sub>G</sub>	Raman shift of D band (cm <sup>-1</sup> )	Raman shift of G band (cm <sup>-1</sup> )	I <sub>D</sub> /I <sub>G</sub>
5%Co–2%Ce/ZrO <sub>2</sub>	1344	1573	0.41	1349	1575	0.40
5%Co–3%Ce/ZrO <sub>2</sub>	1342	1576	0.56	1344	1576	0.55
10%Co–2%Ce/ZrO <sub>2</sub>	1338	1573	0.63	1340	1576	0.62
10%Co–3%Ce/ZrO <sub>2</sub>	1336	1576	0.63	1340	1570	0.62

end of 6 h TOS at 973 K for all tested catalysts. It should be noted that selectivity shifted towards hydrogen with decrease in temperature for the catalysts with 10% Co loading. Additionally, the results indicated that Ce amount, therefore Co/Ce loading ratio, did not have a distinct impact on selectivity at 873 K for the catalysts with the same Co loading.

As the outcome of the abovementioned discussion on reaction conditions, it can be deduced that it is not appropriate to propose an optimum temperature and/or feed ratio due to variation of both extent of primary/secondary reactions [1] in response to reaction conditions and downstream process requirements, especially selectivity, of practical operations.

It was observed after the performance tests that the catalyst bed volume increased due to the deposited carbon whose amount was found dependent on the reaction conditions used; for severe reaction conditions, i.e. for the highest CH<sub>4</sub>/CO<sub>2</sub> ratio, the bed volume was more than quadrupled. Considering the importance of deposited carbon structure on catalyst deactivation, spent catalyst samples were further characterized via Raman spectroscopy. The catalyst samples yielding the highest, at 973 K with CH<sub>4</sub>/CO<sub>2</sub> feed ratio of 2/1, and the moderate, at 873 K with CH<sub>4</sub>/CO<sub>2</sub> feed ratio of 1/1, coke formation were chosen for analysis. Two well-defined bands at around 1340 and 1575 cm<sup>-1</sup> that are attributed to the D band, associated with the disordered structural mode of crystalline carbon species, and G band, corresponding to the graphitic carbon with high degree of symmetry, respectively, were shown at the Raman spectra of spent catalyst samples given in Fig. 16. Thus, graphitic carbon coexisted with amorphous carbon on the surface of all samples at the conditions tested [24,55]. The prevalence of G band on all samples is in accordance with literature since it was stated that graphitic carbon formation is energetically favorable on fcc-Co (111) [55]. The relative intensity of D and G bands (I<sub>D</sub>/I<sub>G</sub>) gives information about the degree of crystallinity; smaller I<sub>D</sub>/I<sub>G</sub> value indicates higher crystallinity. The I<sub>D</sub>/I<sub>G</sub> values were determined as shown in Table 3 for the catalyst samples spent at 873 and 973 K, respectively. Additionally, the graphitization of deposited carbon decreases with reducing metal crystallite size and this phenomenon was also observed in the study of Gurav and co-workers for Ni catalysts [56].

## Conclusions

Co–Ce/ZrO<sub>2</sub> catalysts with different Co/Ce loading ratio were characterized and their performance was parametrically tested under CDRM conditions. Total surface area, pore volume and pore radius values were found comparable in all Co–

Ce/ZrO<sub>2</sub> catalyst samples. Monoclinic zirconia and Co metal with face centered cubic and hexagonal closed packed structures were detected in all samples, and it was shown that Co particles partially cover evenly distributed Ce particles during Co impregnation yielding nonhomogeneous dispersion of Co particles. Higher amount of lattice oxygen vacancies along with the lowest degree of ceria reduction were obtained for 10%Co–2%Ce/ZrO<sub>2</sub> sample, which apparently has the highest Co/Ce ratio. In the performance tests, the extent of side reactions prevailed in determining selectivity profiles of the catalysts. The combined evaluation of characterization and performance results revealed that for the samples having lower Co/Ce ratio, Co–Ce synergistic interaction, that enhances oxygen storage and transfer between species, was stronger, and synchronous contribution of Ce and ZrO<sub>2</sub> to catalytic performance increased. Co/Ce ratio also had an impact on the shape of accumulated carbon and thus affects performance stability of the system. All these findings strongly suggested the possible dominant effect of Co/Ce ratio in CDRM mechanism over the Co–Ce catalysts.

## Acknowledgements

This work is financially supported by TUBITAK through project 111M144. Financial support provided by Republic of Turkey Ministry of Development for laboratory infrastructure and postdoctoral scholarship (Dr. A. I. Paksoy) through project 2016K121160 are greatly acknowledged.

## REFERENCES

- [1] Omogbe O, Danh HT, Nguyen-Huy C, Setiabudi HD, Abidin SZ, Truong QD, et al. Syngas production from methane dry reforming over Ni/SBA-15 catalyst: effect of operating parameters. *Int J Hydrogen Energy* 2017;42:11283–94.
- [2] Li X, Li D, Tian H, Zeng L, Zhao Z, Gong J. Dry reforming of methane over Ni/La<sub>2</sub>O<sub>3</sub> nanorod catalysts with stabilized Ni nanoparticles. *Appl Catal B Environ* 2017;202:683–94.
- [3] Gallego GS, Batiot-Dupeyrat C, Barrault J, Florez E, Mondragon F. Dry reforming of methane over LaNi<sub>1-y</sub>B<sub>y</sub>O<sub>3±δ</sub> (B = Mg, Co) perovskites used as catalyst precursor. *Appl Catal A: Gen* 2008;334:251–8.
- [4] Ballarini A, Basile F, Benito P, Bersani I, Fornasari G, de Miguel S, et al. Platinum supported on alkaline and alkaline earth metal-doped alumina as catalysts for dry reforming and partial oxidation of methane. *Appl Catal A: Gen* 2012;433–434:1–11.

- [5] Luisetto I, Tuti S, Bartolomeo ED. Co and Ni supported on CeO<sub>2</sub> as selective bimetallic catalyst for dry reforming of methane. *Int J Hydrogen Energy* 2012;37:15992–9.
- [6] Jabbour K, Hassan NE, Casale S, Estephane J, Zakhem HE. Promotional effect of Ru on the activity and stability of Co/SBA-15 catalysts in dry reforming of methane. *Int J Hydrogen Energy* 2014;39:7780–7.
- [7] Zhang C, Zhu W, Li S, Wu G, Ma X, Wang X, et al. Sintering-resistant Ni-based reforming catalysts obtained via the nanoconfinement effect. *Catal Commun* 2013;49:9383–5.
- [8] Tian H, Li X, Zeng L, Gong J. Recent advances on the design of group VIII base-metal catalysts with encapsulated structures. *ACS Catal* 2015;5:4959–77.
- [9] Sengupta S, Ray K, Deo G. Effects of modifying Ni/Al<sub>2</sub>O<sub>3</sub> catalyst with cobalt on the reforming of CH<sub>4</sub> with CO<sub>2</sub> and cracking of CH<sub>4</sub> reactions. *Int J Hydrogen Energy* 2014;39:11462–72.
- [10] Ballarini AD, de Miguel SR, Jablonski EL, Scelza OA, Castro AA. Reforming of CH<sub>4</sub> with CO<sub>2</sub> on Pt-supported catalysts effect of the support on the catalytic behavior. *Catal Today* 2005;107–108:481–6.
- [11] Damyanova S, Pawelec B, Arishtirova K, Martinez Huerta MV, Fierro JLG. The effect of CeO<sub>2</sub> on the surface and catalytic properties of Pt/CeO<sub>2</sub>-ZrO<sub>2</sub> catalysts for methane dry reforming. *Appl Catal B: Environ* 2009;89:149–59.
- [12] Alipour Z, Rezaei M, Meshkani F. Effects of support modifiers on the catalytic performance of Ni/Al<sub>2</sub>O<sub>3</sub> catalyst in CO<sub>2</sub> reforming of methane. *Fuel* 2014;129:197–203.
- [13] Li S, Gong J. Strategies for improving the performance and stability of Ni-based catalysts for reforming reactions. *Chem Soc Rev* 2014;43:7245–56.
- [14] Wu G, Li S, Zhang C, Wang T, Gong J. Glycerol steam reforming over perovskite-derived nickel-based catalysts. *Appl Catal B Environ* 2014;144:277–85.
- [15] Xu J, Zhou W, Li Z, Wang J, Ma J. Biogas reforming for hydrogen production over nickel and cobalt bimetallic catalysts. *Int J Hydrogen Energy* 2009;34:6646–54.
- [16] Gould TD, Montemore MM, Lubers AM, Ellis LD, Weimer AW, Falconer JL, et al. Enhanced dry reforming of methane on Ni and Ni-Pt catalysts synthesized by atomic layer deposition. *Appl Catal A: Gen* 2015;492:107–16.
- [17] Sharifi M, Haghighi M, Rahmani F, Karimipour S. Syngas production via dry reforming of CH<sub>4</sub> over Co- and Cu-promoted Ni/Al<sub>2</sub>O<sub>3</sub>-ZrO<sub>2</sub> nanocatalysts synthesized via sequential impregnation and sol-gel methods. *J Nat Gas Sci Eng* 2014;21:993–1004.
- [18] San Jose-Alonso D, Illan-Gomez MJ, Roman-Martinez MC. Low metal content Co and Ni alumina supported catalysts for the CO<sub>2</sub> reforming of methane. *Int J Hydrogen Energy* 2013;38:2230–9.
- [19] Das T, Deo D. Effects of metal loading and support for supported cobalt catalyst. *Catal Today* 2012;198:116–24.
- [20] Ibrahim AA, Fakeeha AH, Al-Fatesh AS. Enhancing hydrogen production by dry reforming process with strontium promoter. *Int J Hydrogen Energy* 2014;39:1680–7.
- [21] Juan-Juan J, Roman-Martinez MC, Illan-Gomez MJ. Effect of potassium content in the activity of K-promoted Ni/Al<sub>2</sub>O<sub>3</sub> catalysts for the dry reforming of methane. *Appl Catal A: Gen* 2006;301:9–15.
- [22] Laosiripojana N, Sutthisripok W, Assabumrungrat S. Synthesis gas production from dry reforming of methane over CeO<sub>2</sub> doped Ni/Al<sub>2</sub>O<sub>3</sub>: influence of the doping ceria on the resistance toward carbon formation. *Chem Eng J* 2005;112:13–22.
- [23] Cheng J, Huang W. Effect of cobalt (nickel) content on the catalytic performance of molybdenum carbides in dry-methane reforming. *Fuel Process Technol* 2010;91:185–93.
- [24] Paksoy AI, Caglayan BS, Aksoylu AE. A study on characterization and methane dry reforming performance of Co-Ce/ZrO<sub>2</sub> catalyst. *Appl Catal B Environ* 2015;168:164–74.
- [25] Khodakov AY. Fischer-Tropsch synthesis: relations between structure of cobalt catalysts and their catalytic performance. *Catal Today* 2009;144:251–7.
- [26] Mahboob S, Haghighi M, Rahmani F. Sonochemically preparation and characterization of bimetallic Ni-Co/Al<sub>2</sub>O<sub>3</sub>-ZrO<sub>2</sub> nanocatalyst: effects of ultrasound irradiation time and power on catalytic properties and activity in dry reforming of CH<sub>4</sub>. *Ultrason Sonochem* 2017;38:38–49.
- [27] Sawabe T, Akiyoshi M, Yoshida K, Yano T. Estimation of neutron-irradiation-induced defect in 3C-SiC from change in XRD peak shift and DFT study. *J Nucl Mater* 2011;417:430–4.
- [28] Renuka L, Anantharaju KS, Sharma SC, Nagaswarupa HP, Prashantha SC, Nagabhushana H, et al. Hollow microspheres Mg-doped ZrO<sub>2</sub> nanoparticles: Green assisted synthesis and applications in photocatalysis and photoluminescence. *J Alloys Compd* 2016;672:609–22.
- [29] Yu P, Zhang K, Huang H, Wen M, Li Q, Zhang W, et al. Oxygen vacancies dependent phase transition of Y<sub>2</sub>O<sub>3</sub> films. *Appl Surf Sci* 2017;410:470–8.
- [30] Miyazawa T, Hanaoka T, Shimura K, Hirata S. Mn and Zr modified Co/SiO<sub>2</sub> catalysts development in slurry-phase Fischer-Tropsch synthesis. *Appl Catal A: Gen* 2013;467:47–54.
- [31] Leppelt P, Schumacher B, Plzak V, Kinne M, Behm RJ. Kinetics and mechanism of the low-temperature water-gas shift reaction on Au/CeO<sub>2</sub> catalysts in an idealized reaction atmosphere. *J Catal* 2006;244:137–52.
- [32] Melchionna M, Fornasiero F. The role of ceria-based nanostructured materials in energy applications. *Mater Today* 2014;17:349–57.
- [33] Deng W, Dai Q, Lao Y, Shi B, Wang X. Low temperature catalytic combustion of 1,2-dichlorobenzene over CeO<sub>2</sub>-TiO<sub>2</sub> mixed oxide catalysts. *Appl Catal B Environ* 2016;181:848–61.
- [34] Fu G, Mao D, Sun S, Yu J, Yang Z. Preparation, characterization and CO oxidation activity of Cu-Ce-Zr mixed oxide catalysts via facile dry oxalate-precursor synthesis. *J Ind Eng Chem* 2015;31:283–90.
- [35] Piumetti M, Bensaid S, Russo N, Fino D. Investigations into nanostructured ceria-zirconia catalysts for soot Combustion. *Appl Catal B Environ* 2016;180:271–82.
- [36] Moses AW, Garcia Flores HG, Kim J, Langell MA. Surface properties of LiCoO<sub>2</sub>, LiNiO<sub>2</sub> and LiNi<sub>1-x</sub>Co<sub>x</sub>O<sub>2</sub>. *Appl Surf Sci* 2007;253:4782–91.
- [37] Holgado JP, Munuera G, Espinos JP, Gonzalez-Elipe AR. XPS study of oxidation processes of CeO defective layers. *Appl Surf Sci* 2000;158:164–71.
- [38] Cai W, Zhong Q, Yu Y, Dai S. Correlation of morphology with catalytic performance of CrO<sub>2</sub>/Ce<sub>0.2</sub>Zr<sub>0.8</sub>O<sub>2</sub> catalysts for NO oxidation via in-situ STEM. *Chem Eng J* 2016;288:238–45.
- [39] Lin SSY, Kim DH, Engelhard MH, Ha SY. Water-induced formation of cobalt oxides over supported cobalt/ceria-zirconia catalysts under ethanol-steam conditions. *J Catal* 2010;273:229–35.
- [40] Chai JW, Pan JS, Wang SJ, Huan CHA, Lau GS, Zheng YB, et al. Thermal behaviour of ultra-thin Co overlayers on rutile TiO<sub>2</sub>(100) surface. *Surf Sci* 2005;589:32–41.
- [41] Watanabe R, Hondo Y, Mukawa K, Fukuhara C, Kikuchi E, Sekine Y. Stable and selective perovskite catalyst for dehydrogenation of propane working with redox mechanism. *J Mol Catal A: Chem* 2013;377:74–84.
- [42] Biesinger MC, Payne BP, Grosvenord AP, Lau LWM, Gerson AR, Smart R. Resolving surface chemical states in XPS analysis of first row transition metals, oxides and

- hydroxides: Cr, Mn, Fe, Co and Ni. *Appl Surf Sci* 2011;257:2717–30.
- [43] Hilmen AM, Schanke D, Hanssen KF, Holmen A. Study of the effect of water on alumina supported cobalt Fischer-Tropsch catalysts. *Appl Catal A: Gen* 1999;186:169–88.
- [44] Wang N, Chu W, Zhang T, Zhao X. Manganese promoting effects on the Co-Ce-Zr-O<sub>x</sub> nano catalysts for methane dry reforming with carbon dioxide to hydrogen and carbon monoxide. *Chem Eng J* 2011;170:457–63.
- [45] Varga E, Ferencz Z, Oszko A, Erdohelyi A, Kiss J. Oxidation states of active catalytic centers in ethanol steam reforming reaction on ceria based Rh promoted Co catalysts: An XPS study. *J Mol Catal A: Chem* 2015;397:127–33.
- [46] Weidler N, Paulus S, Schuch J, Klett J, Hoch S, Stenner P, et al. CoO<sub>x</sub> thin film deposited by CVD as efficient water oxidation catalyst: change of oxidation state in XPS and its correlation to electrochemical activity. *Phys Chem Chem Phys* 2016;18:10708–18.
- [47] Konsolakis M, Sgourakis M, Carabineiro SAC. Surface and redox properties of cobalt-ceria binary oxides: on the effect of Co content and pretreatment conditions. *Appl Surf Sci* 2015;341:48–54.
- [48] Yang J, Liu H, Martens WN, Frost RL. Synthesis and characterization of cobalt hydroxide, cobalt oxyhydroxide, and cobalt oxide nanodiscs. *J Phys Chem C* 2010;114:111–9.
- [49] Nagaoka K, Takanabe K, Aika K. Modification of Co/TiO<sub>2</sub> for dry reforming of methane at 2MPa by Pt, Ru or Ni. *Appl Catal A: Gen* 2004;268:151–8.
- [50] Souza G, Marcilio NR, Perez-Lopez OW. Dry reforming of methane at moderate temperatures over modified Co-Al co-precipitated catalysts. *Mat Res* 2014;17:1047–55.
- [51] Ayodele BV, Khan MR, Cheng CK. Syngas production from CO<sub>2</sub> reforming of methane over ceria supported cobalt catalyst: effects of reactants partial pressure. *J Nat Gas Sci Eng* 2015;27:1016–23.
- [52] Ruckenstein E, Wang HY. Carbon deposition and catalytic deactivation during CO<sub>2</sub> reforming of CH<sub>4</sub> over Co/ $\gamma$ -Al<sub>2</sub>O<sub>3</sub> catalysts. *J Catal* 2002;205:289–93.
- [53] Wolf M, Kotze H, Fischer N, Claeys M. Size dependent stability of cobalt nanoparticles on silica under high conversion Fischer–Tropsch environment. *Faraday Discuss* 2017;197:243–68.
- [54] Liu H, Da Costa P, Taief HBH, Benzina M, Galvez M. Ceria and zirconia modified natural clay based nickel catalysts for dry reforming of methane. *Int J Hydrogen Energy* 2017;42:23508–16.
- [55] de Sousa FF, de Sousa HSA, Oliveira AC, Junioe MCC, Ayala AP, Barros EB, et al. Nanostructured Ni-containing spinel oxides for the dry reforming of methane: effect of the presence of cobalt and nickel on the deactivation behaviour of catalysts. *Int J Hydrogen Energy* 2012;37:3201–12.
- [56] Gurav HR, Dama S, Samuel V, Chilukuri S. Influence of preparation method on activity and stability of Ni catalysts supported on Gd doped ceria in dry reforming of methane. *J CO<sub>2</sub> Util* 2017;20:357–67.